



Spectroscopic Observations of Obscured Populations in the Inner Galaxy: 2MASS-GC02, Terzan 4, and the 200 km s^{-1} stellar peak*

Andrea Kunder¹ , Riley E. Crabb¹, Victor P. Debattista² , Andreas J. Koch-Hansen³ , and Brianna M. Huhmann¹

¹ Saint Martin's University, 5000 Abbey Way SE, Lacey, WA 98503, USA

² Jeremiah Horrocks Institute, University of Central Lancashire, Preston, PR1 2HE, UK

³ Zentrum für Astronomie der Universität Heidelberg, Astronomisches Rechen-Institut, Mönchhofstr. 12-14, D-69120 Heidelberg, Germany

Received 2021 February 25; revised 2021 June 2; accepted 2021 June 4; published 2021 August 3

Abstract

The interpretation of potentially new and already known stellar structures located at low latitudes is hindered by the presence of dense gas and dust, as observations toward these sight lines are limited. We have identified Apache Point Observatory Galaxy Evolution Experiment (APOGEE) stars belonging to the low-latitude globular clusters 2MASS-GC02 and Terzan 4, presenting the first chemical element abundances of stars residing in these poorly studied clusters. As expected, the signature of multiple populations coexisting in these metal-rich clusters is evident. We redetermine the radial velocity of 2MASS-GC02 to be $-87 \pm 7 \text{ km s}^{-1}$, finding that this cluster's heliocentric radial velocity is offset by more than 150 km s^{-1} from the literature value. We investigate a potentially new low-latitude stellar structure and a kiloparsec-scale nuclear disk (or ring) that has been put forward to explain a high-velocity ($V_{\text{GSR}} \sim 200 \text{ km s}^{-1}$) peak reported in several Galactic bulge fields based on the APOGEE commissioning observations. New radial velocities of field stars at $(l, b) = (-6^\circ, 0^\circ)$ are presented and combined with the APOGEE observations at negative longitudes to carry out this search. Unfortunately no prominent -200 km s^{-1} peak at negative longitudes along the plane of the Milky Way are apparent, as predicted for the signature of a nuclear feature. The distances and Gaia EDR3 proper motions of the high- V_{GSR} stars do not support the current models of stars on bar-supporting orbits as an explanation of the $+200 \text{ km s}^{-1}$ peak.

Unified Astronomy Thesaurus concepts: Galactic bulge (2041); Globular star clusters (656); Galaxy kinematics (602); Proper motions (1295); Milky Way formation (1053)

1. Introduction

Mapping the structure of the Galaxy is an essential endeavor, as the Milky Way's (MW's) assembly and star formation history is encoded in the kinematics, metallicities, ages, and spatial distribution of its stars (e.g., Freeman & Bland-Hawthorn 2002; Cooper et al. 2010; Minchev 2016; Helmi et al. 2018). The kinematics and composition of stars in the MW allow for the interpretation of individual components within the Galaxy and relate these to the fundamental properties of galaxy formation models.

The Galactic plane is a region that has remained particularly difficult to probe, as extreme obscuration by interstellar dust and gas, high source density, and confusion with foreground disk populations raise significant limitations in any kind of study (Gonzalez et al. 2012; Nataf et al. 2016; Alonso-García et al. 2018; Nogueras-Lara et al. 2019). Consequently, our view of the inner Galaxy and Galactic bulge is dominated by observations of stars at Galactic latitudes larger than $|b| \sim 2^\circ$.

Modern large surveys using new instrumentation on large telescopes are beginning to penetrate stellar populations that exist also along the plane of the bulge. For example, the infrared photometric VISTA Variables in the Vía Láctea (VVV) ESO Public Survey (Minniti et al. 2010) and the spectroscopic Apache Point Observatory Galaxy Evolution Experiment (APOGEE; Eisenstein et al. 2011) cover large areas of the plane ($|b| < 2^\circ$) of the bulge. This has allowed detailed studies of stars in this populous and crowded region in a more focused fashion.

However, one well-known gap in the literature concerns the population of globular clusters (GCs) in the bulge near the plane of the Galaxy. Surveys such as APOGEE have concentrated more on the GCs in the outskirts of the Galaxy than the bulge (e.g., Mészáros et al. 2020), with the bulge GCs needing to be treated in a more careful manner (e.g., Schiavon et al. 2017; Fernández-Trincado et al. 2019, 2020). This is unfortunate as the bulge GCs are important probes of the formation processes of the central parts of the Galaxy (e.g., Barbuy et al. 2018). There is also a growing debate on the number of globular clusters that exist in the inner Galaxy, as discriminating real from spurious clusters candidates is troublesome (e.g., Froebrich et al. 2007; Gran et al. 2019; Rich et al. 2020).

Another ongoing issue concerns the so-called 200 km s^{-1} peak, which has been reported in the APOGEE fields closest to the plane of the Galaxy. This cold stellar feature ($\sigma_v \sim 35 \text{ km s}^{-1}$) with a galactocentric velocity (V_{GSR}) of $\sim 200 \text{ km s}^{-1}$ was first reported in several Galactic bulge fields based on the APOGEE commissioning observations (Nidever et al. 2012). Nidever et al. (2012) originally proposed that the cold high- V_{GSR} stars are on bar orbits.

Both Li et al. (2014) and Gómez et al. (2016) showed that bar-supporting orbits would produce a high-velocity shoulder, but no discrete peak. Although indeed, many of the APOGEE fields exhibit shoulders and not peaks, 3 of the 53 of the APOGEE fields at positive longitudes do show a discrete V_{GSR} peak with a clear trough (Zhou et al. 2017). For the negative longitudes, Zhou et al. (2021) find no distinct cold high- V_{GSR} peaks in the APOGEE fields, instead finding that complex velocity distributions fit these fields best. However,

* Based on observations taken by APOGEE.

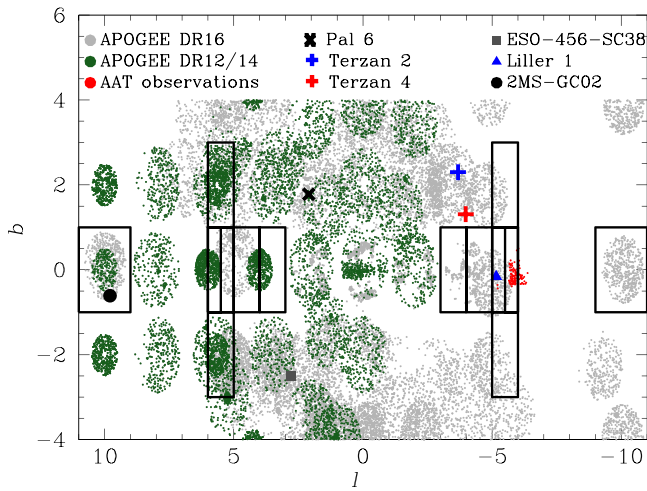


Figure 1. The spatial location of the APOGEE stars included in this study are shown. The grid indicates the spatial division of stars we used to seek for high- V_{GSR} ($|V_{\text{GSR}}| \sim 200 \text{ km s}^{-1}$) peaks. The increase in spectroscopic spatial coverage due to APOGEE DR16 is apparent; in particular, the bulge at negative longitudes can now be explored. Our new AAT observations are shown at $(l, b) = (-6, 0)$, as well as the globular cluster stars included in our analysis.

observations at the negative longitudes are not as extensive or complete, hampering a detailed study.

Aumer & Schönrich (2015) argued that the APOGEE selection function favors young stars, and younger stars would be trapped by the bar into resonant orbits and could give rise to the cool, high-velocity peaks. However, Zasowski et al. (2016), Zhou et al. (2017), and Zhou et al. (2021) showed that stars in the APOGEE high- V_{GSR} peaks do not exhibit distinct chemical abundances or ages, indicating that they are not predominantly comprised of younger stars. Recently, McGough et al. (2020) showed that stars in the propellor orbit family, in isolation, have a kinematic signature similar to that of the 200 km s^{-1} peak.

A further explanation of the cold, high-velocity peak is that the stars in the high- V_{GSR} peak are the signature of a kiloparsec-scale nuclear disk (or ring) that could exist at the center of the Milky Way (Debattista et al. 2015). In this interpretation, the high-velocity peak seen clearly in the APOGEE data at $(l, b) = (6^\circ, 0^\circ)$ is the tangent point of a nuclear structure supported by x_2 orbits, which are perpendicular to the bar (see, e.g., Figure 1 in Debattista et al. 2015). We stress that the kiloparsec-scale nuclear disk put forward by this model is unrelated to the nuclear stellar disk—a dense, disk-like complex of stars and molecular clouds in the nuclear bulge (Launhardt et al. 2002; Nishiyama et al. 2013; Noguerras-Lara et al. 2020) with a radius of $\sim 150 \text{ pc}$.

Here we use the recently released SDSS-IV APOGEE-2 database (Ahumada et al. 2020) supplemented by our own new radial velocities at $(l, b) = (-6^\circ, 0^\circ)$ to search for the signature of the high-velocity peak at negative longitudes. In this way, we can see if there is further supporting evidence of a nuclear feature in the Galaxy. Due to the geometry of the disk, the cold, high-velocity peak should be more pronounced on the $l < 0^\circ$ side if this is due to a nuclear disk or ring (Debattista et al. 2018). Therefore the detection of a high-velocity peak at negative longitudes should be as apparent, if not more, using stars at negative longitudes of the Galaxy.

Unfortunately, very little spectroscopy exists for bulge stars at negative longitudes along the plane of the Milky Way. Trapp

et al. (2018) reported a tentative signature of a ring using SiO masers at $l \sim -8.5^\circ$, but their small sample (~ 140 masers) and large uncertainty in the velocity position prevented a definite conclusion, let alone determining chemical abundances.

In Section 2, we describe the data used in this analysis of the plane of the Galaxy. We test the reliability of using Gaia proper motions in our analysis by considering the proper motions of individual stars belonging to various globular clusters in Section 3. Statistical tests to quantify the signature of a high-velocity peak at negative longitudes are carried in Section 4 and conclusions are given in Section 5.

2. Data

2.1. APOGEE

The APOGEE is a portion of the Sloan Digital Sky Survey (SDSS) III, and has provided a range of data for $\sim 4700 \text{ K/M}$ -giant stars in the MW bulge (Majewski et al. 2016). As APOGEE uses the 2.5 m Sloan telescope in the Northern hemisphere, most of the bulge observed is at positive longitudes. APOGEE is able to collect near-infrared spectra for ~ 300 targets simultaneously. Each of their fields are observed for roughly one hour, which produces high signal-to-noise (S/N) spectra ($S/N > 100$).

Recently, the successor of APOGEE, SDSS-IV APOGEE-2, released new observations of bulge stars (Ahumada et al. 2020). These observations come from the 2.5 m du Pont Telescope at Las Campanas Observatory, using a twin spectrograph to APOGEE (Gunn et al. 2006). The APOGEE observations give estimates of stellar parameters good to $\sim 150 \text{ K}$ for T_{eff} , 0.2 dex for $\log g$, and 0.1 dex for $[\text{Fe}/\text{H}]$, and up to 15 chemical elements have a typical precision of 0.1 dex (García Pérez et al. 2016). The APOGEE data releases comprise the largest near-infrared high-resolution sampling of giant stars of the central region of the Galaxy.

Distances to the APOGEE stars are provided using the the Bayesian isochrone-fitting code StarHorse (Queiroz et al. 2020). This code uses spectroscopic data as well as photometric magnitudes and Gaia parallaxes to derive distance estimates with typical uncertainties of $\sim 6\%$ for APOGEE giants.

To select APOGEE stars that are members of the bulge as opposed to foreground stars, we select those stars with surface gravities of $\log g > 3.8$; this cut is to avoid dwarfs in the foreground. We also require $(J - K_s)_0 > 0.5$ (e.g., Nidever et al. 2012), where we use the AK_TARG value given in APOGEE⁴ and the Nishiyama et al. (2009) extinction law of $A_{K_s} = 0.528 E(J - K_s)$.

The results presented in this paper come from the APOGEE giant stars contained within the grid shown in Figure 1. These observations cover primarily the plane of the inner bulge ($|b| < 1^\circ$). The grid indicates our divisions used in Section 4 (in particular the V_{GSR} histograms shown in Figure 6) to search for potential high- V_{GSR} peaks.

2.2. Anglo-Australian Telescope Observations

One bulge field at $(l, b) = (-6^\circ, 0^\circ)$ was observed on 2020 June 21 (NOAO PropID: 2020A-0368; PI: A. Kunder) using the AAOmega multifiber spectrograph on the Anglo-Australian Telescope (AAT). As this spectrograph is a dual-beam system,

⁴ APOGEE reddening values are calculated using the RJCE method as described in Majewski et al. (2011).

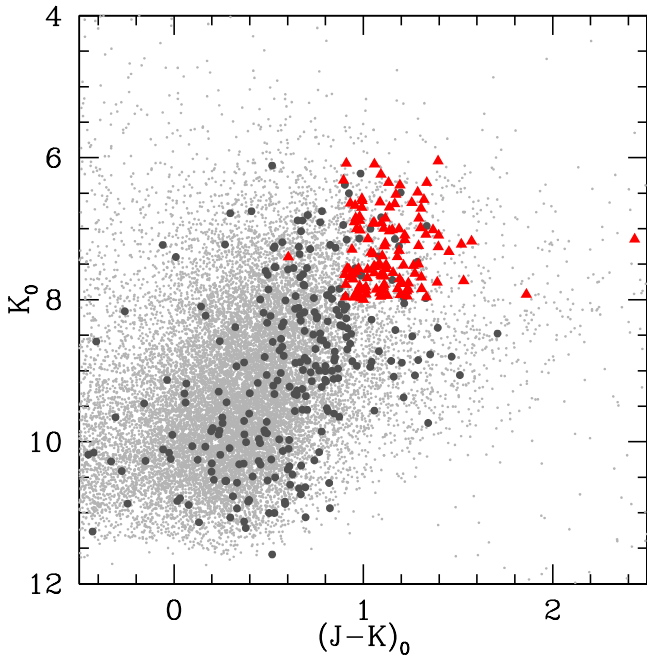


Figure 2. The dereddened 2MASS color–magnitude diagram showing the 130 giants (triangles) for which radial velocities have been determined from AAOmega@AAT. The APOGEE stars observed at $(l, b) = (-5^\circ, 0^\circ)$ are also shown (gray bold points), as are the underlying 2MASS stellar distribution in this field (small gray points). All stars have been dereddened using the extinctions from Gonzalez et al. (2012) and the Nishiyama et al. (2009) extinction law. The uncertainties in the reddening and extinction law dominate the errors in this plot and range from ~ 0.1 – 0.7 mag in both $\Delta E(J - K)$ and ΔA_K .

we used the 580V grating for the Blue arm and the 1700D grating for the Red arm. Due to less than optimal weather conditions, our exposure time was 2×30 minutes, after which the clouds rolled in. Only the spectra from the Red arm were used, as this is where the prominent Calcium Triplet lines could still be distinguished. These spectra covered the wavelength regime of about 8350 \AA – 8850 \AA at a resolution of $R \sim 10,000$.

The automated pipeline supplied by AAOmega, 2dfdr (AAO software Team 2015) was used for the data reduction. Fortunately we were observing during dark time, so despite some cirrus, our sky subtraction was adequate and our spectra ranged in S/N from ~ 1 to 10 per pixel.

The stellar targets were selected from the 2MASS catalog to be located in the $(l, b) = (-6^\circ, 0^\circ)$ region of the sky that had reliable photometric quality indicators e.g., `ph_qual=AAA`. The BEAM extinction calculator (Gonzalez et al. 2012) was used to deredden all stars. Figure 2 shows a clearly defined bulge red giant branch in this field and supports our selection method to target bulge stars. The blue cutoff rejects many objects that are closer than the bulge, which have lower reddening and are brighter than the red giant branch. A number of stars reach the red edge of the RGB, which is where the most metal-rich red giants will fall.

The APOGEE observations in their field 355 + 00 are also shown. Some APOGEE stars fall in a region of the CMD where contamination from the disk and foreground is significant, as also evidenced by their distances that place them primarily either in the foreground or the near side of the bulge (e.g., Queiroz et al. 2020). However, in general, the APOGEE stars also populate the bulge red giant branch uniformly.

The AAT spectra were cross correlated using the IRAF cross-correlation routine, `xcsao`, using the calibration stars taken with the identical setup. Our calibration stars include the following APOGEE stars: 2M18264551-1747096 (HRV = -69.2 km s^{-1}), 2M18255968-174935 (HRV = 49.6 km s^{-1}), 2M18205442-1751063 (HRV = 97.4 km s^{-1}), 2M18235228-1653096 (HRV = -52.7 km s^{-1}), and 2M18233429-1841586 (HRV = 165.8 km s^{-1}), which were observed in a previous observing run (see Kunder et al. 2020a), as well as the APOGEE stars that are located in the same field as our newly observed stars: 2M17342312-3335162 (HRV = -2.2 km s^{-1}) and 2M17340454-3332161 (HRV = -67.3 km s^{-1}). In general, the consistency of our velocity results are 8 km s^{-1} , which is in agreement with the errors reported by `xcsao` for each individual measurement.

3. Globular Clusters

With the Gaia satellite, new astrometric data have become available for approximately a billion stars in the MW galaxy (Gaia Collaboration et al. 2018a, 2021; Lindegren et al. 2020). Combining radial velocities with proper motions from Gaia allows for all three velocity components of stellar motion to be determined. The possibility of using the Gaia proper motions, therefore, completes the measurements of the space motions of a star.

Gaia is ongoing with an anticipated five-year mission lifetime, and the most recent data release (EDR3; Gaia Collaboration et al. 2021) is based on 34 months of observations. Especially in crowded regions of the sky, Gaia faces challenges with astrometric solutions (e.g., Sanders et al. 2019); this will undoubtedly improve by end of mission. Here we corroborate the accuracy of Gaia proper motions in the plane of the Galaxy near the bulge by checking the consistency of the proper motions of stars in GCs. Six globular clusters in the APOGEE footprint located in or close to the plane were used for this purpose; five explored here and one more taken from Kunder & Butler (2020b).

Table 1 lists the individual globular clusters used to verify the reliability of the Gaia EDR3 proper motions. Column 1 is the name of the GC, column 2 lists the average proper motion for the stars selected as cluster candidates, column 3 lists heliocentric distances as reported in the 2010 edition of Harris (1996), column 4 lists the radial velocity of the cluster, and columns 5 and 6 are the published proper motions for the GCs as reported by Rossi et al. (2015) and Vasiliev & Baumgardt (2021), respectively.

Previous papers to isolate globular cluster stars use proper motion as a criterion for membership (e.g., Schiavon et al. 2017; Baumgardt et al. 2019; Vasiliev 2019a; Horta et al. 2020), so we searched for cluster stars in Palomar 6, Terzan 2, Terzan 4, Liller 1, and 2MASS-GC02 using primarily APOGEE radial velocities and the radial distance of a star from the center of the cluster. Also, because globular cluster stars are in general more metal poor than the field population (e.g., Harris 1996; Schiavon et al. 2017; Horta et al. 2020; Mészáros et al. 2020), the metallicities of the stars were used to select candidate cluster members. The published metallicity and radial velocity values for the clusters were used as soft boundaries to guide selection.

Twenty three cluster stars across the five GCs were identified based on their radial velocity, distance from the center of

Table 1
Targeted Globular Cluster Properties

GC	μ_α, μ_δ (This work) (mas yr ⁻¹)	Dist (kpc)	v_r (km s ⁻¹)	μ_α, μ_δ (Rossi et al. 2015) (mas yr ⁻¹)	μ_α, μ_δ (Vasiliev & Baumgardt 2021) (mas yr ⁻¹)
2MASS-GC02	...	7.1	-87	...	$-1.97 \pm 0.16, -3.72 \pm 0.15$
Palomar6	$-9.27 \pm 0.04, -5.34 \pm 0.13$	5.8	181	$2.95 \pm 0.41, 1.24 \pm 0.19$	$-9.20 \pm 0.04, -5.32 \pm 0.03$
Terzan 2	$-2.13 \pm 0.03, -6.34 \pm 0.06$	7.5	109	$0.94 \pm 0.30, 0.15 \pm 0.42$	$-2.17 \pm 0.04, -6.25 \pm 0.04$
Terzan 4	$-5.21 \pm 0.15, -3.61 \pm 0.07$	7.2	-50	$3.50 \pm 0.69, 0.35 \pm 0.58$	$-5.62 \pm 0.07, -3.62 \pm 0.07$
Liller 1	$-5.34 \pm 0.14, -7.37 \pm 0.12$	8.1	52	...	$-5.40 \pm 0.13, -7.48 \pm 0.10$
ESO 456-SC38 ^a	$0.73 \pm 0.04, -3.06 \pm 0.07$	8.8	-150	$3.08 \pm 0.29, 2.00 \pm 0.34$	$0.67 \pm 0.04, -2.99 \pm 0.03$

Notes.

^a from Kunder & Butler (2020b), updated EDR3 proper motions.

Table 2
Parameters and Abundances of Globular Cluster Stars

APOGEE ID	RV	r	Distance	μ_α	μ_δ	[Fe/H]	[C/Fe]	[N/Fe]	[Na/Fe]	[Mg/Fe]	[Al/Fe]
2MASS-GC02											
2M18092967-2048019	-83.018	0.442	-1.108	-0.013	0.239	0.290	0.397	-0.274
2M18092981-2045283	-96.486	0.305
2M18093270-2046243	-96.398	0.161
2M18093410-2047235	-82.504	0.242	...	-0.966	-0.837
2M18093595-2045134	-81.327	0.173
2M18093761-2047483	-79.247	0.302	-0.874	-0.172	1.083	-0.752	0.213	0.619
2M18093935-2046378	-87.985	0.153	-1.019	-0.200	0.860	0.344	0.058	0.217
Palomar 6											
2M17433738-2612050	170.807	0.724	7.271	-9.275	-5.480	-0.767	-0.192	0.891	0.391	0.274	0.278
2M17433806-2613426	170.652	0.640	6.370	-9.328	-4.922	-0.911	-0.136	0.343	0.159	0.283	0.078
2M17434071-2613528	178.616	0.501	7.292	-9.114	-5.707	-1.070	0.008	0.111	...	0.344	-0.147
2M17434331-2610217	175.957	1.177	...	-9.302	-5.258	-0.887	-0.069	0.124	0.310	0.379	0.070
2M17434675-2616068	175.716	1.480	6.710	-9.351	-5.330	-0.799	-0.083	0.699	0.360	0.309	0.168
Terzan 2											
2M17273185-3048156	132.974	0.366	...	-2.094	-6.309	-0.763	-0.085	0.909	0.047	0.259	0.282
2M17273364-3047243	131.310	0.835	...	-2.170	-6.459	-0.775	-0.101	0.909	0.290	0.340	0.202
2M17273419-3048097	133.152	0.405	...	-2.079	-6.194	-0.874	-0.057	0.619	0.044	0.329	0.042
2M17273540-3047308	135.249	0.967	...	-2.191	-6.414	-0.877	-0.007	0.115	-0.018	0.422	0.067
Terzan 4											
2M17302949-3135089	-47.944	1.917	...	-4.991	-3.480	-1.414	-0.285	0.528	0.147	0.248	-0.019
2M17303796-3135329	-52.774	0.309	...	-5.159	-3.719	-1.292	-0.255	0.867	0.519	0.011	0.721
2M17303838-3135492	-44.255	0.117	...	-5.488	-3.644	-1.442	-0.314	0.214	...	0.250	-0.258
Liller1											
2M17332090-3322320	68.586	1.425	4.249	-5.374	-7.245
2M17332272-3323206	71.754	0.494	...	-4.551	-7.259
2M17332472-3323166	56.550	0.119	...	-5.805	-7.250
2M17332881-3322499	49.152	1.284	...	-5.645	-7.714	-0.578	0.149	0.319	...	0.305	-0.036

cluster, and, when available, metallicity. Table 2 lists the individual stars in each targeted globular cluster, as well as the radial velocity and the elemental abundances [Fe/H], [C/Fe], [N/Fe], [Na/Fe], [Mg/Fe], and [Al/Fe] of the star as reported by APOGEE DR16. The distances in column 4 are from StarHorse, taken directly from Queiroz et al. (2020). While APOGEE stars in the cluster Palomar 6 were studied previously in Schiavon et al. (2017) and Mészáros et al. (2020), we still carried out a selection of stars in this cluster. This was to avoid any kind of potential proper motion biases that would artificially lower the scatter in the average proper motions of these stars. We present the first APOGEE stars in the globular clusters 2MASS-GC02, Terzan 4 and Liller 1.

3.1. 2MASS-GC02

Figure 3 shows an example of the selection of APOGEE stars in an understudied GC, 2MASS-GC02 (Hurt et al. 2000).

An overdensity of stars close to the center of the cluster with radial velocities of ~ -87 km s⁻¹ and metallicities of [Fe/H] ~ -1.0 is apparent. These are likely not field stars, but instead almost certainly belong to 2MASS-GC02. Curiously Borissova et al. (2007) present 15 stars with S/N > 30 that lie within 1'3 of 2MASS-GC02 and that have colors and magnitudes consistent with the giant branch of 2MASS-GC02. From 12 of these stars, they find an average radial velocity of $\sim -238 \pm 36$ km s⁻¹. However, Figure 3 shows no stars with such large radial velocities.

The right panel of Figure 3 shows that our seven candidate 2MASS-GC02 stars also have colors and magnitudes consistent with being members of the cluster. The reddening of this cluster is extreme, $A_V > 15$ mag or $E(J - K_s) = 3.1 \pm 0.5$ mag (Hurt et al. 2000; Ivanov et al. 2000), and it has been noted that the extinction toward this cluster is highly variable (up to 50% change in extinction over small regions) and with significant deviations from the standard extinction law (Alonso-García

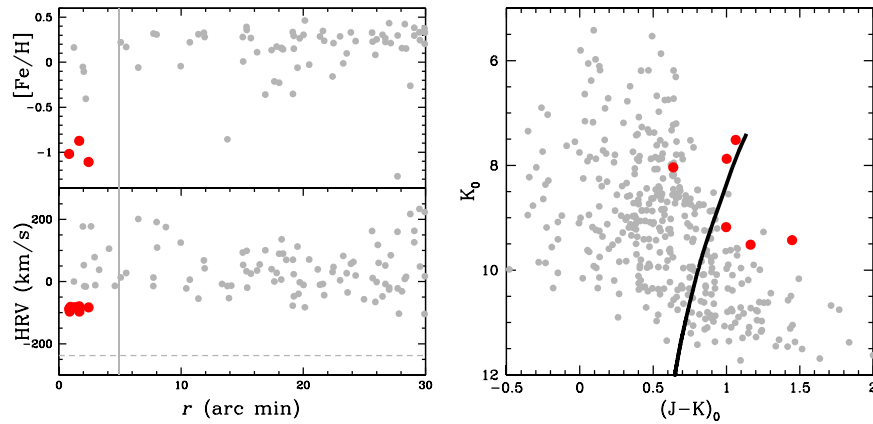


Figure 3. The heliocentric velocity (bottom left) and $[\text{Fe}/\text{H}]$ metallicity (top left) of APOGEE stars within $30'$ of 2MASS-GC02. The tidal radius of $r_t = 4'9$ is shown, as is the radial velocity of the cluster as derived from Borissova et al. (2007). The color–magnitude diagram of the same stars is shown in the right panel. The clump of seven stars with radial velocities of -87 km s^{-1} at a distance of $1'$ from the center of the cluster are consistent with being cluster stars. The solid black line shows the BaSTI isochrone that best matches the cluster’s observed parameters (see text). The APOGEE uncertainties in $[\text{Fe}/\text{H}]$ are $0.1\text{--}0.2$ dex, the APOGEE uncertainties in radial velocity are $<0.5 \text{ km s}^{-1}$, and the uncertainties in the dereddened CMD range from $\sim 0.1\text{--}0.7$ mag in both $\Delta E(J-K)$ and ΔA_K .

et al. 2015). Peñaloza et al. (2015) have found the stars in this cluster are α enhanced, as is typical of old globular clusters in the bulge (e.g., Dias et al. 2016; Mészáros et al. 2020; Horta et al. 2020). The BaSTI (Pietrinferni et al. 2004, 2006) α -enhanced stellar evolution models⁵ were adopted to indicate the approximate location of the red giant branch of 2MASS-GC02. We used the publicly available BaSTI isochrone that best matches the cluster’s observed parameters, one with an age of 12.5 Gyr, a metallicity of $[\text{Fe}/\text{H}] = -1.01$ dex, and a distance modulus of $(m - M)_0 = 13.48$ mag (Borissova et al. 2007).

It therefore seems likely that the seven stars we identified as being cluster members of 2MASS-GC02 are bona fide cluster members and redetermine the radial velocity of 2MASS-GC02 to be $-87 \pm 7 \text{ km s}^{-1}$. Unfortunately, only one of the seven stars has a Gaia proper motion so our sample to check for proper motion consistency is not sufficient.

It is important to stress that our selection differs from that of Baumgardt et al. (2019), Vasiliev (2019a), and Vasiliev & Baumgardt (2021), who used the distribution of sources in proper motion space as a parameter to select cluster members. These authors then determined the mean proper motions of almost the entire known population of Milky Way GCs. Because proper motion is not used as a selection criterion for isolating cluster stars here, we can then find the scatter in the proper motions of our selected GC stars. We use this as an indicator of the reliability of Gaia proper motions in a typical sample of APOGEE stars residing in the most crowded regions of the inner Galaxy.

Figure 4 shows the individual proper motions of the cluster stars identified here. In general, the average values of cluster stars we selected (without using proper motion criteria) have a proper motion scatter of $\sim 0.15 \text{ mas yr}^{-1}$ or less. This value is in agreement with the average uncertainty in proper motion found in Vasiliev & Baumgardt (2021), also using globular cluster stars. Although the absolute proper motion values for the clusters are consistent with the values presented by Baumgardt et al. (2019) and Vasiliev (2019a), they are not consistent with the absolute proper motion values presented in Rossi et al. (2015), which are computed using field stars as an absolute reference frame. The Rossi et al. (2015) proper motion

values dramatically differ in the zero point by $3\text{--}11 \text{ mas yr}^{-1}$, and no correlation between the Gaia EDR3 proper motions and those presented by Rossi et al. (2015) are apparent. Although systematic errors in Gaia proper motions have been reported (e.g., Vasiliev 2019b; Lindegren et al. 2018; Gaia Collaboration et al. 2018b), offsets of $>1 \text{ mas yr}^{-1}$ are not thought to be likely.

3.2. Chemical Element Abundances

Observational evidence demonstrates that most Galactic GCs host (at least) two main groups of stars with different chemical composition. One population of stars, referred to as the first generation, have a similar chemical composition as halo field stars with similar metallicity, while the other population of stars have enhanced helium, nitrogen, and sodium abundances, but are depleted in carbon and oxygen (e.g., Kraft 1994; Carretta et al. 2009; Marino et al. 2019). The origin of these multiple populations is still an open issue (e.g., Gratton et al. 2012; Renzini et al. 2015; Bastian & Lardo 2018).

GCs in the inner Galaxy represent a moderately metal-rich population and are thought to be some of the oldest GCs in the Galaxy (e.g., VandenBerg et al. 2013; Massari et al. 2019). However, bulge GCs are less studied than those in the halo, as high and often variable extinction, as well as crowding and the difficulty in separating true bulge stars from intervening thin and thick disk stars, makes them more difficult to analyze in detail (e.g., Bica et al. 2016). Whereas almost all GCs studied have shown signs of multiple populations with certain dependencies on mass (and age), it is less clear how $[\text{Fe}/\text{H}]$ metallicity affects the multiple-population phenomena (Kayser et al. 2008; Carretta et al. 2009; Hanke et al. 2017; Bastian & Lardo 2018). For example, old, metal-rich clusters have been found that do not exhibit multiple populations (e.g., Salinas & Strader 2015) and these clusters have been used to suggest improvement in the models of GC formation (Tang et al. 2017).

This paper is the first to present the APOGEE stars and their chemical element abundances in the clusters 2MASS-GC02 and Terzan 4. As such, a search for multiple populations in these clusters is carried out. Due to the small numbers of stars per cluster with elemental abundances, we are hesitant to carry out a deeper analysis, e.g., identifying gaps in the elemental distribution or identifying clusters that are chemically

⁵ <http://basti-iac.oa-abruzzo.inaf.it>

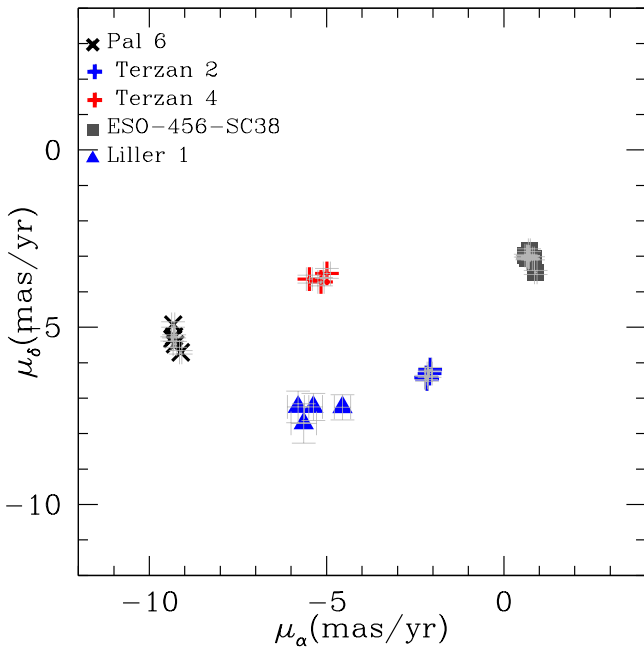


Figure 4. The proper motion distribution for globular cluster stars in APOGEE selected using radial velocity, metallicity, and distance from the cluster center. The formal errors on the proper motions as reported by Gaia are indicated by thin gray lines and are typically smaller than the size of the symbols. The Gaia EDR3 proper motions are stable also in crowded bulge regions, e.g., within 2.5 degrees from the plane of the Galaxy.

analogous. A few days after this paper was accepted, the bulge Cluster APOgee Survey (CAPOS), carried out a study on Terzan 4, finding a similar result to what is presented here (Geisler et al. 2021).

Figure 5 shows the elemental abundances of C, N, Na, Al, and Mg of our candidate cluster stars. In all these clusters (except for Liller 1 for which we have only one star with an APOGEE elemental abundance), a widespread in elemental abundances is seen, indicative of multiple stellar populations. Despite small number statistics for our clusters, the C–N anticorrelation is apparent as is the Mg–Al anticorrelation. For example, we have only three stars in Terzan 4 with APOGEE elemental abundances, but their spread in $[Al/Fe]$ ranges from ~ -0.25 to $\sim +0.75$ dex and their spread in $[N/Fe]$ ranges from ~ 0.2 to ~ 0.8 dex. For all clusters studied here, stars with enhanced $[N/Fe]$ abundances populate the cluster. These peculiar chemical patterns appear to be ubiquitous for almost all GCs studied properly and are also typical of stars in bulge clusters (e.g., Schiavon et al. 2017; Nataf et al. 2019; Fernández-Trincado et al. 2019, 2020).

Some of the cluster stars are considerably aluminum enhanced, with $[Al/Fe] > +0.5$, but still exhibit low levels of magnesium (e.g., $[Mg/Fe] < 0.2$). This abundance pattern is similar to the ~ 30 chemical peculiar APOGEE field stars reported toward the bulge region by Fernández-Trincado et al. (2020). Their speculation that these aluminum enhanced metal-poor stars originated from GCs and were dynamically ejected into the bulge is supported by our observations of aluminum enhanced stars in the inner bulge GCs.

4. The 200 km s^{-1} Peak

As discussed in the introduction, Nidever et al. (2012) identified cold velocity peaks in the radial velocity distribution

of stars within $\sim 20^\circ$ of the Galactic Center. Many of these peaks were shown to not be statistically significant (Zhou et al. 2017) and there has also been the suggestion that APOGEE’s selection function was biased (Aumer & Schönrich 2015). Other studies have shown that some of these velocity peaks or shoulders can be associated with resonant bar orbits (Molloy et al. 2015; McGough et al. 2020). It has also been suggested that the most prominent velocity peak at $(l, b) = (6^\circ, 0^\circ)$ is caused by stars moving on x_2 orbits in a kiloparsec-sized nuclear disk or ring (Debattista et al. 2015, 2018).

4.1. Velocity Distributions

When Nidever et al. (2012) first reported the so-called 200 km s^{-1} peak at positive longitudes along the plane of the Galaxy, there were no observations at the negative longitudes to search for a counterfeature (see Figure 1). This was unfortunate, because its prominence (or “peakiness”) and how widespread it is at negative longitudes, could help discriminate between scenarios which attempt to explain this feature. For example, if the counterfeature is widespread and appears as a shoulder instead of a discrete peak, this would agree with the models put forth by e.g., Li et al. (2014), Aumer & Schönrich (2015), Gómez et al. (2016), and Zhou et al. (2021) that the 200 km s^{-1} peak is composed of stars on bar-supporting orbits. If the counterfeature is confined to longitudes between $1 \sim 6^\circ$ and $1 \sim 8^\circ$ and is a discrete peak, this would agree with the suggestion of Debattista et al. (2018) that the 200 km s^{-1} peak is composed of stars belonging to a nuclear disk or ring.

Figure 6 shows the galactocentric velocities for the APOGEE DR16 at negative longitudes compared to those from APOGEE DR12/DR14 for the positive longitudes. Our new observations described in Section 2 are also folded in, as they provide a more direct comparison to the $(l, b) = (6^\circ, 0^\circ)$ field than using the APOGEE DR16 observations alone, as there are no APOGEE stars at longitudes between $+6^\circ$ and $+7^\circ$.

A nuclear feature would be present mainly within $b \pm 1^\circ$ and also mainly around $|l| \sim 5^\circ\text{--}8^\circ$, as this is the line-of-sight tangent to the nuclear disk/ring (e.g., see Figure 1; Debattista et al. 2015). The left panel of Figure 6 concentrates on this region of the bulge. The right panel shows the velocity distributions for stars at longitudes reaching to $|l| = +10^\circ$ and $|l| = 2.5^\circ$ as well as fields $\pm 2^\circ$ from the plane of the Galaxy. Any high- V_{GSR} features/signatures in these fields would not be due to a nuclear feature in these off-plane fields.

A potential counterpeak at $\sim 200 \text{ km s}^{-1}$ appears to become more prominent and more separated from the rest of the distribution as the observations approach $|l| = 6^\circ$, but the $1 \sim +6^\circ$ observations show a significantly more pronounced peak as compared to at $1 \sim 6^\circ$. Our radial velocity distributions show that stars do occupy the high- V_{GSR} regime also around $(l, b) = (-5.5^\circ, 0^\circ)$, but there is no obvious negative high- V_{GSR} peak.

Figure 7 shows the APOGEE DR16 combined with the AAT velocities for 312 stars in the field centered on $(l, b) = (-5.5^\circ, 0^\circ)$. A Shapiro–Wilk test for normality on the radial velocity distribution gives p -values < 0.05 , indicating that the radial velocity distribution formally deviates from a Gaussian distribution. A k -means clustering algorithm is used to determine where the radial velocity distribution is aggregated. A 4 peak curve provides the best fit to the $(l, b) = (-5.5^\circ, 0^\circ)$

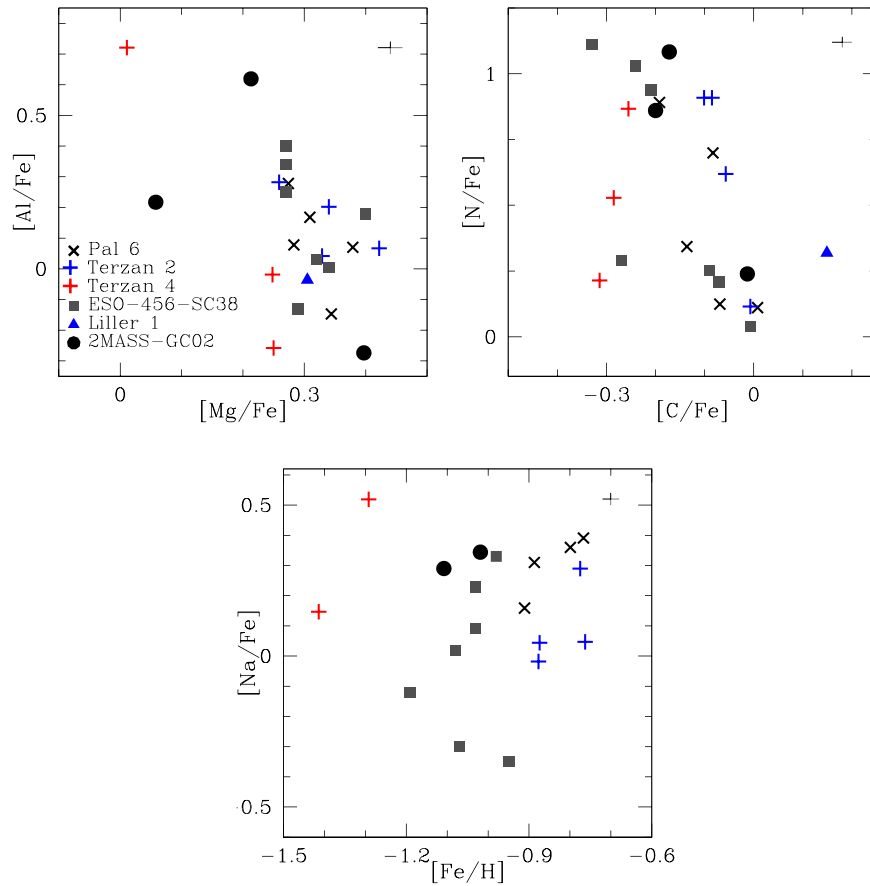


Figure 5. The APOGEE chemical abundances for C, N, Na, Al, and Mg in the cluster stars presented here. The formal uncertainty in the APOGEE elemental abundances is indicated in the top right. All clusters show a widespread of elemental abundances, indicating multiple populations coexist within these bulge clusters.

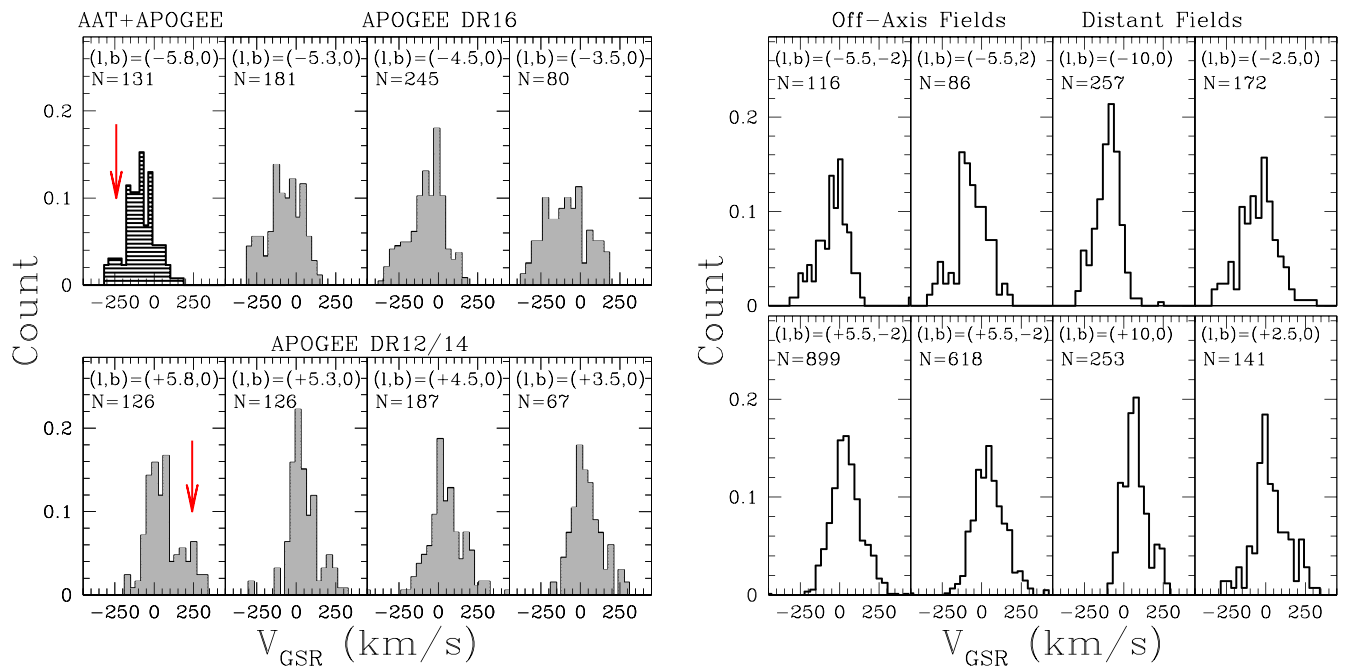


Figure 6. The Galactocentric velocities of the APOGEE DR16 observations along the plane at negative longitudes along the plane (top) are compared to the APOGEE DR12/DR14 observations at positive longitudes (bottom). For the $(l, b) = (-5.8, 0)$ field, our new AAT observations have been folded in. No strong ~ -200 km s $^{-1}$ counterfeature to the $(l, b) = (5.8, 0)$ field is apparent. The arrows indicate where the expected high V_{GSR} would be if these stars were part of a kiloparsec-sized nuclear disk. Right: The Galactocentric velocities of the APOGEE observations in off-axis fields and along the plane where there should be no apparent nuclear feature.

velocity distribution and a Gaussian mixture model (GMM) indicates that the radial velocity peaks are at $[-45$ km s $^{-1}$,

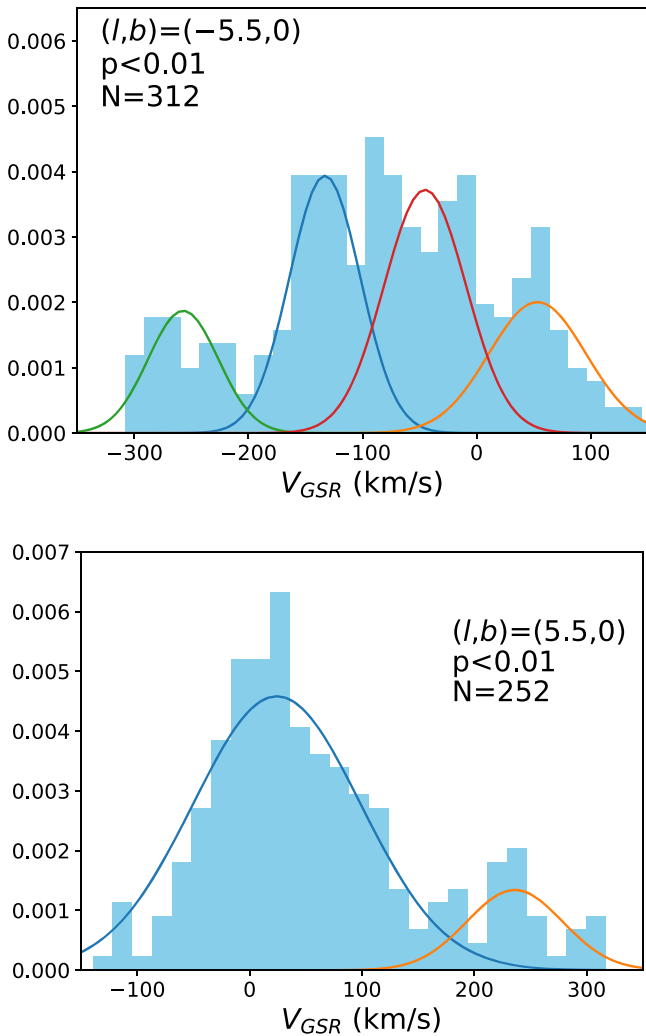


Figure 7. A histogram of the Galactocentric velocities of APOGEE stars at $(l, b) = (5.5, 0^\circ)$ (bottom) and the APOGEE+AAT stars at $(l, b) = (-5.5, 0^\circ)$ (top). The best-fit curve to the histogram from a k -means clustering algorithm and a GMM is overlaid. The mean and standard deviations of these distributions are given in Table 3.

-133 km s^{-1} , 53 km s^{-1} , -257 km s^{-1}] with dispersions of $[36 \text{ km s}^{-1}$, 31 km s^{-1} , 43 km s^{-1} , $31 \text{ km s}^{-1}]$ and weights of $[0.34, 0.31, 0.21, 0.14]$, respectively.

This can be compared to the velocities of 252 stars in the field centered on $(l, b) = (5.5, 0^\circ)$. In this field, a 2 peak curve provides the best fit to the velocity distribution, and a GMM indicates that the radial velocity peaks are at $[24 \text{ km s}^{-1}$, $236 \text{ km s}^{-1}]$ with dispersions of $[75 \text{ km s}^{-1}$, $43 \text{ km s}^{-1}]$ and weights of $[0.86, 0.14]$, respectively. Whereas the $(l, b) = (-5.5, 0^\circ)$ shows a complicated distribution of velocities, the $(l, b) = (5.5, 0^\circ)$ field exhibits a clear double peak, with one of the main peaks being at a positive high V_{GSR} . That the bulge velocity distribution is complex is not surprising given the large velocity dispersions reported especially in bulge fields close to the Galactic plane (e.g., Kunder et al. 2012), and that the bulge is made up of a complex variety of stellar populations coexisting in the central regions of the MW (e.g., Recio-Blanco et al. 2017; Queiroz et al. 2020; Rojas-Arriagada et al. 2020 and references therein).

Table 3 lists the Shapiro–Wilk p -value, the number of peaks computed from k -means, and the GMM values of where the

peaks are located for the fields shown in Figure 7. Although formally these statistical tests provide a quantitative characterization of the velocity distribution of stars near the plane of the Galaxy, we believe the large velocity dispersion combined with the sample size makes it difficult to conclusively determine the underlying velocity distribution.

It is evident that any preference for an excess of stars at $V_{\text{GSR}} \sim -200 \text{ km s}^{-1}$ in the $l = -5.5$ field is not as extreme as was seen in the $l = +5.5$ field, nor is it confined to only this field. For example, the field at $(l, b) = (-10^\circ, 0^\circ)$ and at $(l, b) = (-4^\circ, 0^\circ)$ also may show some indication for a $V_{\text{GSR}} \sim -200 \text{ km s}^{-1}$ peak.

The Figure 6 presented here is similar to the velocity distributions shown in (Zhou et al. 2021, their Figure 2), except that we have ~ 100 more stars with radial velocities centered on $(l, b) = (-6^\circ, 0^\circ)$ due to our new AAT observations. We also show velocity histograms spanning ranges of longitude to specifically explore a counterfeature at negative longitudes. Instead of selecting 2° fields based on where the positive longitude fields are centered, we separate the stars so they naturally follow the sparser coverage along the negative longitudes (see Figure 1). In particular, as there is no negative longitude field centered on $(l, b) = (-6^\circ, 0^\circ)$, we do not show a velocity distribution for this field. Instead, the $(l, b) = (-5.5, 8.0^\circ)$ field presented here spans half a degree from -5.5 to -6.0 and the $(l, b) = (-5.5, 3.0^\circ)$ field spans half a degree from -5.0 to -5.5 . These fields can be directly compared to the APOGEE stars at positive longitudes and hence more closely mirrors the APOGEE observations in hand.

4.2. Velocity and Distance Correlations

Li et al. (2014) and Zhou et al. (2017) use MW simulations to remark that in a distance-velocity diagram, higher-velocity particles should be at larger distances. This is due to the geometric intersections between the line of sight and the particles orbit; at the tangent points of a star’s orbit, it will have the highest velocity and remain there longer relative to us. The StarHorse distances (Queiroz et al. 2020) released for the APOGEE DR16 stars can be used to explore if the high-velocity stars seen in the histograms presented above are consistent with particle motions in an axisymmetric disk.

Figure 8 shows the velocity distributions for those stars with StarHorse distances between 4 and 6 kpc compared to the velocity distributions for those stars with distances >6 kpc. In both fields there are still stars with distances between 4 and 6 kpc that occupy the high- V_{GSR} peaks. There is only a mild trend for stars with on average larger distances to have larger velocities. The stars with distances between 4 and 6 kpc have dominant velocity peaks at $\sim |50| \text{ km s}^{-1}$. In contrast, stars with distances larger than 6 kpc are not as strongly peaked and instead have tails extending to larger velocities. This suggests that the high- V_{GSR} peak cannot be explained by stars at larger distances alone, although it may also be that the StarHorse distances are not reliable for these stars. The plane of the Galaxy has especially high and variable extinction values and this may affect the accuracy of the StarHorse distances.

4.3. Velocity and Proper-motion Correlations

Gaia proper motions are available for a number of stars along the plane and in Section 3 we showed that they can be used also in this crowded region of the Galaxy. In particular, from an

Table 3
Statistical Properties of the APOGEE Velocity Distributions

Field	l Range	b Range	Num Stars	# Gaussians	Mean	Sigma	Weight	Data
$(l,b) = (-10, 0)$	-11:-9	-1:1	257	2	-71, -177	59, 67	0.70, 0.30	APOGEE DR16
$(l,b) = (-5.5, 0)$	-6:-5	-1:1	312	4	-45, -133, 53, -257	36, 31, 43, 31	0.34, 0.31, 0.21, 0.14	APOGEE + AAT
$(l,b) = (-5.5, 0)$	-6:-5	-1:1	220	4	-31, -122, 57, -256	29, 34, 34, 30	0.29, 0.33, 0.22, 0.15	APOGEE
$(l,b) = (-5.8, 0)$	-6:-5.5	-1:1	131	4	-53, -140, 49, -260	37, 29, 54, 33	0.39, 0.32, 0.17, 0.12	APOGEE + AAT
$(l,b) = (-5.3, 0)$	-5.5:-5	-1:1	181	4	-121, -30, 57, -255	34, 29, 35, 30	0.34, 0.26, 0.24, 0.16	APOGEE DR16
$(l,b) = (-5.5, -2)$	-6:-5	-3:-1	116	2	-25, -101	73, 162	0.70, 0.30	APOGEE DR16
$(l,b) = (-5.5, 2)$	-6:-5	1:3	86	3	-87, 43, -254	43, 56, 39	0.55, 0.32, 0.13	APOGEE DR16
$(l,b) = (-4.5, 0)$	-5:-4	-1:1	245	2	-24, -209	76, 76	0.72, 0.28	APOGEE DR16
$(l,b) = (-3.5, 0)$	-4:-3	-1:1	80	3	-62, -222, 94	54, 62, 46	0.42, 0.37, 0.21	APOGEE DR16
$(l,b) = (-2, 0)$	-3:-1	-1:1	401	4	-99, 4, 129, -228	47, 47, 74, 52	0.37, 0.33, 0.16, 0.15	APOGEE DR16
$(l,b) = (+2, 0)$	1:3	-1:1	477	3	8.7, 148, -126	53, 71, 60	0.49, 0.30, 0.21	APOGEE DR16
$(l,b) = (+3.5, 0)$	3:4	-1:1	67	2	2, 144	62, 77	0.73, 0.27	APOGEE DR12/14
$(l,b) = (+4.5, 0)$	4:5	-1:1	187	2	32, 108	83, 160	0.72, 0.28	APOGEE DR12/14
$(l,b) = (+5.3, 0)$	5:5.5	-1:1	126	3	18, 144, -137	44, 80, 119	0.66, 0.29, 0.05	APOGEE DR12/14
$(l,b) = (+5.8, 0)$	5.5:6	-1:1	126	2	19, 233	71, 50	0.79, 0.21	APOGEE DR12/14
$(l,b) = (+5.5, 0)$	5:6	-1:1	252	2	24, 236	75, 43	0.86, 0.14	APOGEE DR12/14
$(l,b) = (+5.5, -2)$	6:5	-3:-1	899	2	16, 92	74, 112	0.63, 0.37	APOGEE DR16
$(l,b) = (+5.5, 2)$	6:5	1:3	618	2	8.2, 117	82, 94	0.63, 0.37	APOGEE DR16
$(l,b) = (+10, 0)$	9:11	-1:1	253	2	50, 158	57, 125	0.75, 0.25	APOGEE DR12/14

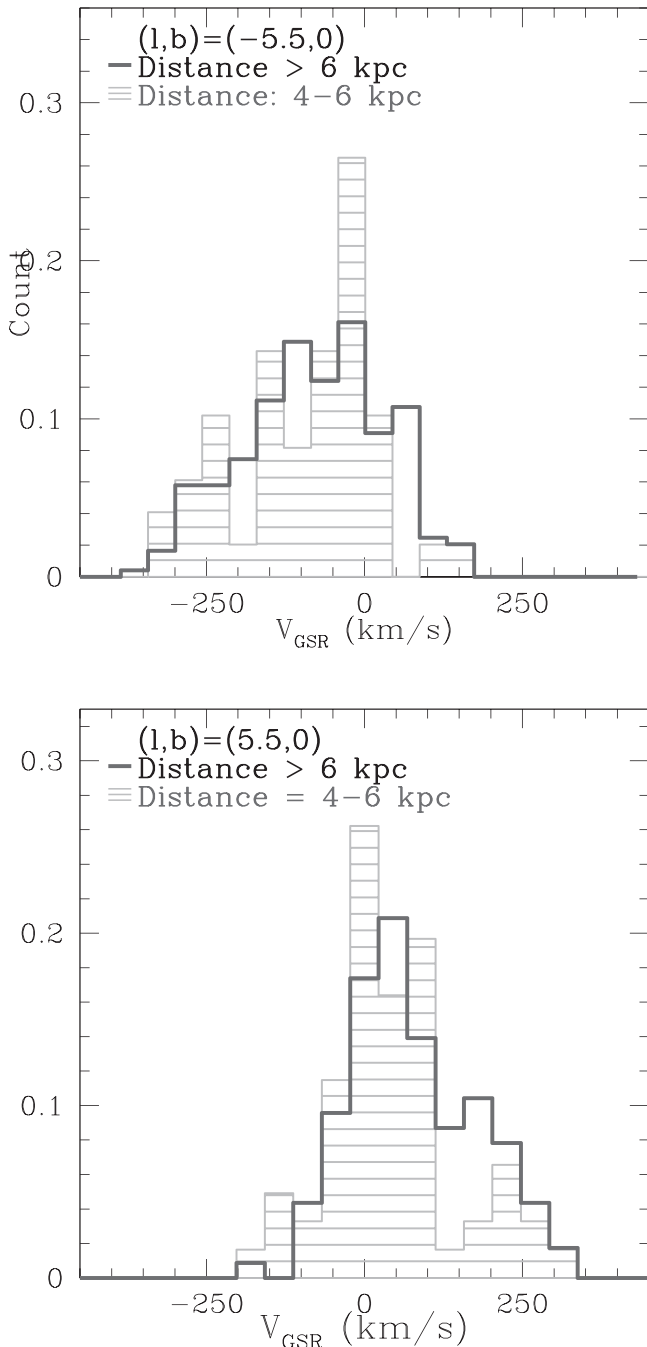


Figure 8. The Galactocentric velocity distribution of APOGEE Stars -6° field (top) and the $+6^\circ$ field (bottom) separated by heliocentric distance. In general, stars with larger distances (solid line) have larger velocities.

analysis of globular cluster stars, a star-to-star scatter of 0.15 mas yr^{-1} or less can be expected. Formally the precision of the EDR3 proper motions is $\sim 0.07 \text{ mas yr}^{-1}$ (at $G = 17$) for Gaia EDR3 as compared to 0.2 mas yr^{-1} (at $G = 17$) in Gaia DR2 (Lindgren et al. 2020). Gaia EDR3 proper motions offer not only an increase in precision, but the number of stars with proper motions along the plane also increases by $\sim 15\%$ as compared to Gaia DR2. Therefore, our sample of stars along the plane is useful to probe the correlation between the high- V_{GSR} regime also in proper-motion space.

Figure 9 shows the correlation between velocity and μ_ℓ for 249 stars at $(l, b) = (5.5, 0^\circ)$. At a velocity of

$V_{\text{GSR}} > 100 \text{ km s}^{-1}$, stars have proper motions with larger $|\mu_\ell|$ values than the rest of the sample. In particular, stars with $> 100 \text{ km s}^{-1}$ have μ_ℓ of $\sim -7.5 \text{ mas yr}^{-1}$ as compared to μ_ℓ of -4 mas yr^{-1} for the bulge field.

The μ_ℓ for 328 stars at $(l, b) = (-5.5, 0^\circ)$ shows the same trend for the positive high- V_{GSR} stars—the stars with $\sim 200 \text{ km s}^{-1}$ velocities have $|\mu_\ell|$ proper motions larger than the rest of the sample. In contrast, the negative high- V_{GSR} stars have a similar μ_ℓ to the bulge field. There is no preponderance for the negative high- V_{GSR} regime to have different μ_ℓ proper motions to the bulge field.

The same trend in proper motion is also seen $\pm 2^\circ$ from the plane. There is no indication that the stars along the plane of the Galaxy at $|l| = 5.5$ differ in μ_ℓ as compared to those $\pm 2^\circ$ from the plane at $|l| = 5.5$.

McGough et al. (2020) use 71 stars at $l \sim 6^\circ$, 52 stars at $l \sim 8^\circ$ and 27 stars at $l \sim 4^\circ$ to show that the high- V_{GSR} stars occupy a smaller range in μ_ℓ than the full sample of stars. They attribute this to stars on periodic orbits in an exponential bar, such as propeller orbits. They were not able to investigate the proper motions at negative longitudes. Zhou et al. (2021) corroborate the result from McGough et al. (2020) result using DR2 proper motions for the APOGEE DR16 sample. Here we are able to offer additional insights on the correlation between velocity and μ_ℓ in the bulge using the better precision and sampling of the EDR3 proper motions combined with both the APOGEE and our new AAT observations.

Besides Gaia proper motions, proper motions of bulge stars from Smith et al. (2018) are publicly available through the VIRAC catalog, a near-infrared proper motion and parallax catalog of the VISTA Variables in the VVV survey. Out of the 3614 APOGEE stars within $|b| < 1^\circ$, $(J - K)_0 > 0.5$ and $\log g > 3.8$, about half of those (1656) have a VIRAC proper motion and about a third of those (592) have a flag = 1, indicating it is reliable. In particular, in the $(-5.5, 0)$ field, there are 220 stars with VIRAC proper motions and in the $(+5.5, 0)$ field there are 98 stars with VIRAC proper motions. This overlap is smaller than when using Gaia EDR3. There are 1510 APOGEE stars within $|b| < 1^\circ$, $(J - K)_0 > 0.5$ and $\log g > 3.8$ that have a Gaia EDR3 proper motion; 87% of these have absolute proper motion uncertainties $< 1 \text{ mas yr}^{-1}$. The number of APOGEE stars with Gaia proper motions in the $(-5.5, 0)$ and $(5.5, 0)$ field is greater by a factor of 1.5–2.

Using the VIRAC, proper motions result in the same trends as seen above in Figure 9 using the more extensive Gaia EDR3 proper motions. APOGEE stars with radial velocities of $\sim 200 \text{ km s}^{-1}$ have larger $|\mu_\ell|$ values. This is the case both for the bulge stars with $|b| < 1^\circ$ as well as the stars at $|b| \sim 2^\circ$.

We prefer not to combine the Gaia and VIRAC proper motion catalogs due to the offsets between these catalogs caused by the drift motion of the pool of reference stars used for each pawprint set in VIRAC (see e.g., Smith et al. 2018; Clarke et al. 2019). These are estimated to be $+2.20 \text{ mas yr}^{-1}$ in μ_α and $-4.85 \text{ mas yr}^{-1}$ in μ_δ ; the authors mention it is quite probable that there are unknown systematic uncertainties besides these offsets as well.

5. Discussion

Proper motions from Gaia EDR3, radial velocities from APOGEE, distances from StarHorse, and our own observations from the AAT are combined for stars along the plane of the Galaxy with the aim of testing the hypothesis that the

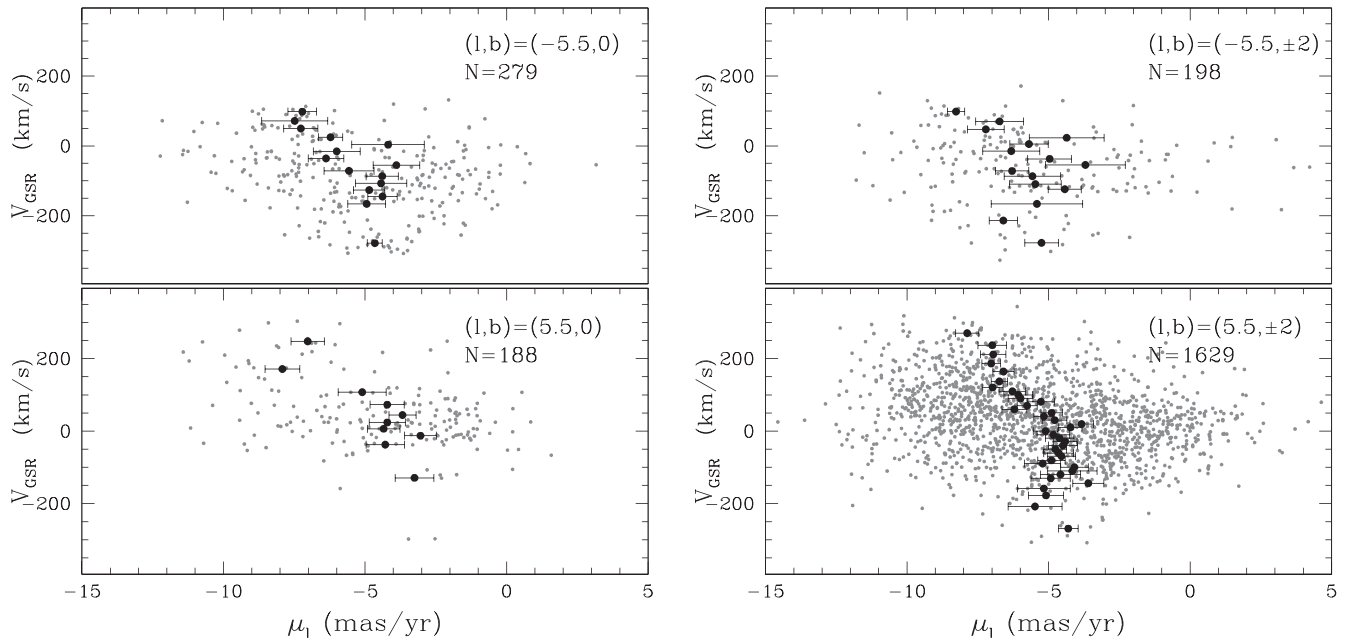


Figure 9. The V_{GSR} velocities as a function of proper motion, μ_ℓ , for the fields at positive (top) and negative (bottom) longitudes. Whereas the positive high- V_{GSR} stars have proper motions offset from the rest of the bulge, this is not the case for the negative high- V_{GSR} stars.

high- V_{GSR} stars are the signature of a nuclear disk or ring (Debattista et al. 2018). Our new observations from the AAT at $(l,b) = (-6^\circ, 0^\circ)$ are combined with the APOGEE DR16 observations to increase the sample size of stars with radial velocities at negative longitudes where the tangent point of a nuclear feature should be evident.

From a GMM analysis the putative negative high- V_{GSR} peak at $(l,b) = (-5^\circ.5, 0^\circ)$ is at $V_{\text{GSR}} \sim -250 \text{ km s}^{-1}$ whereas the positive high- V_{GSR} peak at $(l,b) = (5^\circ.5, 0^\circ)$ is at $V_{\text{GSR}} \sim 230 \text{ km s}^{-1}$. Therefore, the negative high- V_{GSR} stars have the larger $|V_{\text{GSR}}|$, in contrast to what is expected for a nuclear feature.

Along the plane of the Galaxy, the new Gaia EDR3 proper motions increase the number of APOGEE stars with proper motions by $\sim 15\%$ as compared to Gaia DR2. The proper motions of the high- V_{GSR} stars occupy a small range in proper motions, spanning $\sim 5 \text{ mas yr}^{-1}$. This is inconsistent with what is predicted for stars in a nuclear feature, as proper motions of stars in both a nuclear disk and nuclear ring would span a wider range of in μ_ℓ , $\sim 10 \text{ mas yr}^{-1}$ (Debattista et al. 2018).

The μ_ℓ of the positive high V_{GSR} exhibit larger $|\mu_\ell|$ proper motions than the bulge stars. However, the negative high- V_{GSR} stars have similar μ_ℓ proper motions as bulge stars. Zhou et al. (2021) argues that this observed $V_{\text{GSR}}-\mu_\ell$ distribution is consistent with the predictions of a simple MW bar model as presented in Shen et al. (2010). This is especially the case if the APOGEE stars were to lie predominantly in front of the Galactic Center. However, the Shen et al. (2010) model does not predict a distinct peak at $(l,b) = (5^\circ.5, 0^\circ)$. The only way to produce this peak in the Shen et al. (2010) model is if the high- V_{GSR} stars are at distances at $\sim 8.5 \pm 1 \text{ kpc}$ (see e.g., Figure 3 in Li et al. 2014). Accordingly there is a tension in the Shen et al. (2010) model between the APOGEE stars needing to be at $\sim 8.5 \text{ kpc}$ to explain any high- V_{GSR} peak but to be primarily in front of the Galactic center to match the μ_ℓ proper motions.

Although there are negative high- V_{GSR} stars residing in the negative longitude fields, the negative high- V_{GSR} peak is not nearly as prominent or discrete as seen in the positive high- V_{GSR} peak at the positive longitudes (see Figure 6). Stars on propellor orbits as described by McGough et al. (2020) are not able to explain this. The propellor orbits can produce positive high- V_{GSR} stars with similar proper motions to what is observed, but there is no reason why APOGEE would select just these orbits at $(l,b) = (5^\circ.5, 0^\circ)$. Although it has been hypothesized that the APOGEE selection function preferably selects young stars (Aumer & Schönrich 2015), stars on propellor orbits would not necessarily be young and there has been no observational evidence to suggest that high- V_{GSR} stars are in fact younger than the bulk of the population (Zasowski et al. 2016; Zhou et al. 2017, 2021). Therefore, those propellor orbits would give rise to a strong secondary peak only at $(l,b) = (5^\circ.5, 0^\circ)$, which is not a satisfactory way of explaining a distinct high- V_{GSR} peak.

It was shown in (e.g., Li et al. 2014) the high- V_{GSR} stars can be explained by stars at larger distances, although this would produce a high- V_{GSR} peak instead of a shoulder. Using StarHorse distances we are not able to confirm that the high- V_{GSR} stars are at further distances. This leaves open a different interpretation for the peak in the APOGEE high- V_{GSR} stars than current MW models of the orbits of bulge stars suggest.

Our analysis assumes that the completeness between APOGEE-2 and APOGEE for the bulge fields are similar without major differences in the selection effects. This is the case for other studies using APOGEE DR16 to compare the positive and negative longitudes of the inner galaxy (e.g., Zhou et al. 2021; Rojas-Arriagada et al. 2020). Zasowski et al. (2017) report that in both APOGEE-2 and APOGEE, bulge giants are selected based on their dereddened $(J-K)$ colors, requiring $(J-K)_0 > 0.5$, and Figure 2 shows no obvious indication that the APOGEE stars at negative longitudes do not probe the full $(J-K)_0$ color range for bulge giants. Although, there have

been no detailed investigations to investigate selection effects in APOGEE DR16 (see e.g., Nandakumar et al. 2017; Fragkoudi et al. 2018). Queiroz et al. (2021) uses cartesian density maps of the bulge stars to surmise that the complex mix of stellar populations and selection function of APOGEE does provide a homogeneous coverage of the entire inner Galaxy. Fortunately, the detection of a high-velocity peak at negative longitudes should be as apparent, if not more, using stars at negative longitudes of the Galaxy (Debattista et al. 2018). Yet still, our different cuts and stellar divisions within the APOGEE-2 data set (e.g., Figures 6 and 7; Table 3) do not show any obvious -200 km s^{-1} peak.

6. Conclusions

The APOGEE DR16 observations combined with Gaia EDR3 proper motions are used to investigate the hypothesis that the cold high-velocity peak (at $V_{\text{GSR}} \sim 200 \text{ km s}^{-1}$; Nidever et al. 2012) are due to a kiloparsec nuclear feature (Debattista et al. 2015, 2018). The APOGEE DR16 data in the negative longitudes were examined for a counterpeak at $V_{\text{GSR}} \sim -200 \text{ km s}^{-1}$. Some evidence for a high-velocity shoulder in a number of different APOGEE negative longitude fields along the plane is seen, but no dominant $V_{\text{GSR}} \sim -200 \text{ km s}^{-1}$ feature is apparent. Unfortunately the sample size is small compared to the large velocity dispersion of the bulge population along the plane of the Galaxy and a larger sample size as well as wider coverage (e.g., $l = -6^\circ$ to -8°) would offer a deeper view on characterizing any $\sim |200| \text{ km s}^{-1}$ feature. Distances and proper motions of the high-velocity stars are inconsistent with the $\sim |200| \text{ km s}^{-1}$ stars belonging to different classes of bar orbits from model for galactic bars as put forth by previous investigations (e.g., Li et al. 2014; Zhou et al. 2017; McGough et al. 2020; Zhou et al. 2021). They are also inconsistent with the idea that the MW harbors a kiloparsec nuclear feature (Debattista et al. 2015, 2018). We therefore currently have no single model that can explain the high- V_{GSR} observations.

To corroborate the accuracy of the Gaia EDR3 proper motions along the plane of the Galaxy, APOGEE stars in a number of globular clusters are identified without the aid of proper motion criteria. Many of these stars had previously not been reported. The first APOGEE stars in the globular clusters 2MASS-GC02 and Terzan 4 are presented, both of which show evidence of multiple populations. The average radial velocity of the stars in 2MASS-GC02 is $-87 \pm 7 \text{ km s}^{-1}$, which is more than 150 km s^{-1} offset from the literature value (Borissova et al. 2007).

We thank the referee for suggestions that improved the quality of our analysis. A.M.K and R.E.C. are thankful to colleagues Danielle Miller and Andrew Schulz for aiding with the AAT observations and for stimulating conversations. A.M. K. acknowledges support from grant AST-2009836 from the National Science Foundation. The grant support provided, in part, by the M.J. Murdock Charitable Trust (NS-2017321) is acknowledged. V.P.D. is supported by STFC Consolidated grant #ST/R000786/1. A.J.K-H gratefully acknowledges funding by the Deutsche Forschungsgemeinschaft (DFG, German Research Foundation)—Project-ID 138713538—SFB 881 (“The Milky Way System”), subprojects A03, A05, A11.

ORCID iDs

Andrea Kunder  <https://orcid.org/0000-0002-2808-1370>
 Victor P. Debattista  <https://orcid.org/0000-0001-7902-0116>
 Andreas J. Koch-Hansen  <https://orcid.org/0000-0002-9859-4956>

References

- AAO software Team 2015, 2drdf: Data reduction software, Astrophysics Source Code Library, ascl:1505.015
- Ahumada, R., Allende Prieto, C., Almeida, A., et al. 2020, *ApJS*, 249, 3
- Alonso-García, J., Saito, R. K., Hempel, M., et al. 2018, *A&A*, 619, 4
- Alonso-García, J., Dékány, I., Catelan, M., et al. 2015, *AJ*, 149, 99
- Aumer, M., & Schönrich, R. 2015, *MNRAS*, 454, 3166
- Barbuy, B., Chiappini, C., & Gerhard, O. 2018, *ARA&A*, 56, 223
- Bastian, N., & Lardo, C. 2018, *ARA&A*, 56, 83
- Baumgardt, H., Hilker, M., Sollima, A., & Bellini, A. 2019, *MNRAS*, 482, 5138
- Bica, E., Barbuy, B., & Ortolani, S. 2016, *PASA*, 33, 28
- Borissova, J., Ivanov, V. D., Stephens, A. W., et al. 2007, *A&A*, 474, 121
- Carretta, E., Bragaglia, A., Gratton, R., & Lucatello, S. 2009, *A&A*, 505, 139
- Clarke, J. P., Wegg, C., Gerhard, O., et al. 2019, *MNRAS*, 489, 3519
- Cole, D. R., Debattista, V. P., Erwin, P., Earp, S. W. F., & Roskar, R. 2014, *MNRAS*, 445, 3352
- Cooper, A. P., Cole, S., Frenk, C. S., et al. 2010, *MNRAS*, 406, 744
- Debattista, V. P., Ness, M., Earp, S. W. F., & Cole, D. R. 2015, *ApJ*, 812, L16
- Debattista, V. P., Earp, S. W. F., Ness, M., & Gonzalez, O. A. 2018, *MNRAS*, 473, 5275
- Dias, B., Barbuy, B., Saviane, I., et al. 2016, *A&A*, 590, 9
- Eisenstein, D. J., Weinberg, D. H., Agol, E., et al. 2011, *AJ*, 142, 72
- Fernández-Trincado, J. G., Zamora, O., Souto, D., et al. 2019, *A&A*, 627, 178
- Fernández-Trincado, J. G., Minniti, D., Beers, T. C., et al. 2020, *A&A*, 643, 145
- Fernández-Trincado, J. G., Beers, T. C., Minniti, D., et al. 2020, *A&A*, 643, 4
- Fragkoudi, F., Di Matteo, P., Haywood, M., et al. 2018, *A&A*, 616, 180
- Freeman, K., & Bland-Hawthorn, J. 2002, *ARA&A*, 40, 487
- Froebich, D., Meusinger, H., Scholz, A., Raftery, C. L., & Davis, C. J. 2007, *AN*, 328, 701
- Gaia Collaboration, Brown, A. G. A., Vallenari, A., et al. 2018a, *A&A*, 616, A1
- Gaia Collaboration, Helmi, A., van Leeuwen, F., et al. 2018b, *A&A*, 616, A12
- Gaia Collaboration, Brown, A. G. A., Vallenari, A., et al. 2021, *A&A*, 649, A1
- García Pérez, A. E., Allende Prieto, C., Holtzman, J. A., et al. 2016, *AJ*, 151, 144
- Geisler, D., Villanova, S., O’Connell, J. E., et al. 2021, arXiv:2106.00024
- Gómez, A., Di Matteo, P., Stefanovitch, N., et al. 2016, *A&A*, 589, 122
- Gonzalez, O. A., Rejkuba, M., Zoccali, M., et al. 2012, *A&A*, 543, 13
- Gran, F., Zoccali, M., Contreras Ramos, R., et al. 2019, *A&A*, 628, 45
- Gratton, R. G., Carretta, E., & Bragaglia, A. 2012, *A&ARv*, 20, 50
- Gunn, J. E., Siegmund, W. A., Mannery, E. J., et al. 2006, *AJ*, 131, 2332
- Harris, W. E. 1996, *AJ*, 112, 1487
- Helmi, A., Babusiaux, C., Koppelman, H. H., et al. 2018, *Natur*, 563, 85
- Hanke, M., Koch, A., Hansen, C. J., & McWilliam, A. 2017, *A&A*, 599, 97
- Horta, D., Schiavon, R. P., Mackereth, J. T., et al. 2020, *MNRAS*, 493, 3363
- Hurt, R. L., Jarrett, T. H., Kirkpatrick, J. D., et al. 2000, *AJ*, 120, 1876
- Ivanov, V. D., Borissova, J., & Vanzì, L. 2000, *A&A*, 362, 1
- Kayser, A., Hilker, M., Grebel, E. K., & Willemsen, P. G. 2008, *A&A*, 486, 437
- Kazantzidis, S., Bullock, J. S., Zentner, A. R., Kravtsov, A. V., & Moustakas, L. A. 2008, *ApJ*, 688, 254
- Kraft, R. P. 1994, *PASP*, 106, 553
- Kunder, A., Koch, A., Rich, R. M., et al. 2012, *AJ*, 143, 57
- Kunder, A. M., Pérez-Villegas, A., Rich, R. M., et al. 2020a, *AJ*, 159, 270
- Kunder, A. M., & Butler, E. 2020b, *AJ*, 160, 241
- Launhardt, R., Zylka, R., & Mezger, P. G. 2002, *A&A*, 384, 112
- Li, Z.-Y., Shen, J., Rich, R. M., Kunder, A., & Mao, S. 2014, *ApJL*, 785, L17
- Lindgren, L., Hernandez, J., Bombrun, A., et al. 2018, *A&A*, 616, 2
- Lindgren, L., Klioner, S. A., Hernandez, J., et al. 2020, *A&A*, 616, 2
- Majewski, S. R., Zasowski, G., & Nidever, D. L. 2011, *ApJ*, 739, 25
- Majewski, S. R. & APOGEE Team 2016, *AN*, 337, 863
- Marino, A. F., Milone, A. P., Renzini, A., et al. 2019, *MNRAS*, 487, 3815
- Martínez-Valpuesta, I., & Gerhard, O. 2011, *ApJL*, 734, L20
- Massari, D., Koppelman, H. H., & Helmi, A. 2019, *A&A*, 630, 4
- McGough, D. P., Evans, N. W., & Sanders, J. L. 2020, *MNRAS*, 493, 2676

- Mészáros, S., Masseron, T., & García-Hernández, D. A. 2020, *MNRAS*, **492**, 1641
- Minchev, I. 2016, *AN*, **337**, 703
- Minniti, D., Lucas, P. W., Emerson, J. P., et al. 2010, *NewA*, **15**, 433
- Molloy, M., Smith, M. C., Evans, N. W., & Shen, J. 2015, *ApJ*, **812**, 146
- Nandakumar, G., Schultheis, M., Hayden, M., et al. 2017, *A&A*, **606**, 97
- Nataf, D. M., Gonzalez, O. A., Casagrande, L., et al. 2016, *MNRAS*, **456**, 2692
- Nataf, D. M., Wyse, R., Schiavon, R. P., et al. 2019, *AJ*, **158**, 1
- Nidever, D. L., Zasowski, G., Majewski, S. R., et al. 2012, *ApJ*, **755**, L25
- Nishiyama, S., Tamura, M., Hatano HI Kato, D., et al. 2009, *ApJ*, **696**, 1407
- Nishiyama, S., Yasui, K., Nagata, T., Yoshikawa, T., Uchiyama, H., et al. 2013, *ApJ*, **769**, 28
- Nogueras-Lara, F., Schödel, R., Gallego-Calvente, A. T., et al. 2019, *A&A*, **630**, 3
- Nogueras-Lara, F., Schödel, R., Gallego-Calvente, A. T., et al. 2020, *NatAs*, **4**, 377
- Peñaloza, F., Pessev, P., Vázquez, S., et al. 2015, *PASP*, **127**, 329
- Pérez-Villegas, A., Barbuy, B., Kerber, L. O., et al. 2020, *MNRAS*, **491**, 3251
- Pietrinferni, A., Cassisi, S., Salaris, M., & Castellì, F. 2004, *ApJ*, **612**, 167
- Pietrinferni, A., Cassisi, S., Salaris, M., & Castellì, F. 2006, *ApJ*, **642**, 797
- Portail, M., Wegg, C., Gerhard, O., & Martínez-Valpuesta, I. 2015, *MNRAS*, **448**, 713
- Queiroz, A. B. A., Anders, F., Chiappini, C., et al. 2020, *A&A*, **638**, 76
- Queiroz, A. B. A., Chiappini, C., Pérez-Villegas, A., et al. 2021, arxiv:2007.12915
- Recio-Blanco, A., Rojas-Arriagada, A., de Laverny, P., et al. 2017, *A&A*, **602**, L14
- Renzini, A., D’Antona, F., Cassisi, S., et al. 2015, *MNRAS*, **454**, 4197
- Rich, R. M., Johnson, C. I., Young, M., et al. 2020, *MNRAS*, **499**, 2340
- Rojas-Arriagada, A., Zasowski, G., Schultheis, M., et al. 2020, *MNRAS*, **499**, 1037
- Rossi, L. J., Ortolani, S., Barbuy, B., Bica, E., & Bonfanti, A. 2015, *MNRAS*, **450**, 3270
- Salinas, R., & Strader, J. 2015, *ApJ*, **809**, 169
- Sanders, J. L., Smith, L., & Evans, N. W. 2019, *MNRAS*, **488**, 4552
- Schiavon, R. P., et al. 2017, *MNRAS*, **465**, 501
- Shen, J., Rich, M. R., Kormendy, J., et al. 2010, *ApJL*, **720**, L72
- Smith, L. C., Lucas, P. W., Kurtev, R., et al. 2018, *MNRAS*, **474**, 1826
- Tang, B., Cohen, R. E., Geisler, D., et al. 2017, *MNRAS*, **465**, 19
- Trapp, A. C., Rich, R. M., Morris, M. R., et al. 2018, *ApJ*, **861**, 75
- VandenBerg, D. A., Brogaard, K., Leaman, R., & Casagrande, L. 2013, *ApJ*, **775**, 134
- Vasiliev, E. 2019a, *MNRAS*, **484**, 2832
- Vasiliev, E. 2019b, *MNRAS*, **489**, 623
- Vasiliev, E., & Baumgardt, H. 2021, *MNRAS*, **505**, 5978
- Zasowski, G., Ness, M. K., García Pérez, A. E., et al. 2016, *ApJ*, **832**, 132
- Zasowski, G., Cohen, R. E., Chojnowski, S. D., et al. 2017, *AJ*, **854**, 198
- Zhou, Y., Shen, J., Liu, C., et al. 2017, *ApJ*, **847**, 74
- Zhou, Y., Liu, Z. Y., Simion, I., et al. 2021, *ApJ*, **908**, 21